Investigation of Collective Fast Ion Instability-induced Redistribution or Loss in the National Spherical Torus Experiment

S. S. Medley 1), R. Andre 1), R. E. Bell 1), D. S. Darrow 1), E. D. Fredrickson 1), B. P. LeBlanc 1), F. M. Levinton 2), J. E. Menard 1), D. Stutman 3), A. L. Roquemore 1), K. Shinohara 4), K. Tritz 3), H. Yuh 2) and the NSTX Research Team

1) Princeton Plasma Physics Laboratory, Princeton University, Princeton, NJ 08543 USA
2) Nova Photonics, Inc., Princeton, NJ 08543 USA
3) Johns Hopkins University, Baltimore, Maryland, USA
4) Japan Atomic Energy Agency, Naka, Ibaraki 311-0193, Japan

Main author email contact: medley@pppl.gov

Abstract. The National Spherical Torus Experiment (NSTX) is particularly well suited to investigate fast-ion driven instabilities because large values of the dimensionless parameters $v_{fast}/v_{Alfvén}$ and $\beta_{fast}(0)/\beta_{tot}(0)$ required to drive such instabilities occur routinely in neutral beam heated plasmas. The instabilities can be divided into three categories; chirping Energetic Particle Modes (EPM) in the frequency range 0 – 120 kHz, the Toroidal Alfvén Eigenmodes (TAE) with a frequency range of 50 – 200 kHz and the Global and Compressional Alfvén Eigenmodes (GAE and CAE, respectively) between 300 kHz and the ion cyclotron frequency. These modes are of particular interest because of their potential to cause substantial fast ion redistribution or loss. Both the volume-integrated neutron and the line-integrated charge exchange neutral particle diagnostics show signal depletion due to fast-ion driven instabilities, but cannot distinguish between fast-ion redistribution or loss. Two recently implemented diagnostics on NSTX, the Motional Stark Effect (MSE) and scintillator Fast Lost Ion Probe (sFLIP), facilitate separation of redistribution and loss effects. Outward redistribution of the core-peaked energetic beam ions modifies the beam-driven current profile and hence the core q-profile. MSE-constrained q-profiles are being used to assess this effect. sFLIP measures the pitch and energy of fast ions that are ejected from the plasma and intercept the wall-mounted probe thus identifying fast-ion loss. For certain H-mode discharges where NPA measurements of the NB energetic ion spectra exhibit MHD-induced fast-ion depletion, the sFLIP data confirm the existence of an ion loss that occurs primarily for passing particles near the NB full injection energy. Observations and TRANSP simulations representing fast ion instability-induced redistribution/loss phenomena in NSTX are presented.

1. Introduction

The physics of plasmas that contain large populations of super-Alfvénic energetic particles is an important outstanding issue for burning plasma experiments, such as ITER. The National Spherical Torus Experiment (NSTX) is particularly well suited to investigate fast-ion driven instabilities and their influence on fast particle confinement, since the Neutral Beam Injection (NBI) heated plasmas can match or exceed the ITER dimensionless parameter regime for $v_{fast}/v_{Alfvén}$ and $\beta_{fast}(0)/\beta_{tot}(0)$ as demonstrated in Fig. 1 (albeit at much higher fast-ion ρ^*).

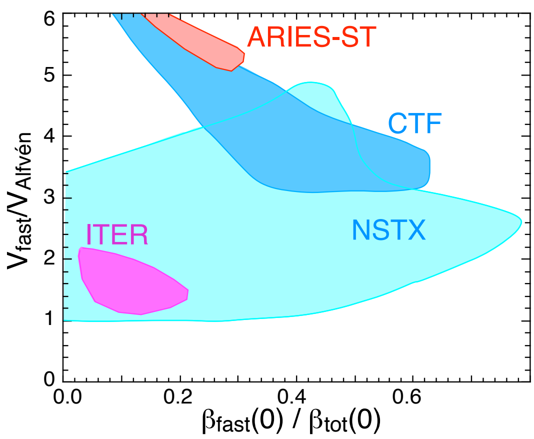

Fig. 1 Diagram showing the operating boundaries of NSTX, ITER, CTF and ARIES-ST in the dimensionless fast particle parameters $v_{fast}/v_{Alfvén}$ and $\beta_{fast}(0)/\beta_{tot}(0)$

As illustrated by the Mirnov spectrogram shown in Fig. 2, a wide variety of fast ion driven instabilities, some recently discovered, are excited during high-power NBI in NSTX.

TAEs [1] and other Alfvén eigenmodes [2] are destabilized when the fast-ion velocity v_b is larger than the Alfvén speed v_A. The modes can be divided into three categories; chirping Energetic Particle Modes (EPM) in the frequency range 0 – 120 kHz, the Toroidal Alfvén Eigenmodes (TAE) with a frequency range of 50 – 200 kHz and the Global and Compressional Alfvén Eigenmodes (GAE and CAE, respectively) between 300 kHz and the ion cyclotron frequency. Some of the higher frequency modes exhibit a frequency splitting characteristic of what would be expected from "hole-clump" theory [3]. The TAEs can appear either as saturated modes or as bursting modes and the bursting TAEs observed in NSTX [4] can cause significant fast ion losses. Compressional Alfvén modes (CAE) have a frequency scaling, polarization, dependence on the fast-ion distribution function, and low frequency limit that are qualitatively consistent with CAE theory. Thus far, CAE and GAE modes do not appear to cause fast ion loss in NSTX.

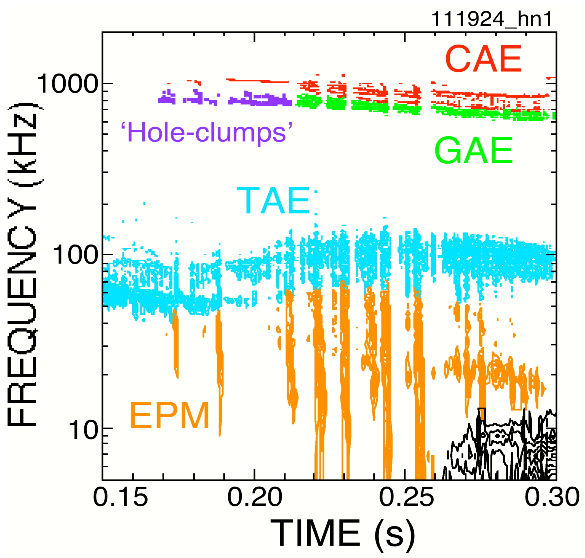

Fig. 2 Mirnov spectrogram of a neutral beam heated shot on NSTX showing the wide variety of fast particle modes.

In addition to Alfvénic modes, energetic ion redistribution/loss associated with low frequency kink-type magnetohydromagnetic (MHD) activity has been observed [5]. Outward redistribution of the core-peaked energetic beam ions can modify the NBI-driven current profile and hence the core q-profile, as reported for Alfvénic modes in DIII-D [6,7] and MHD modes in NSTX [8]. In this work, TRANSP [9] simulations using space, energy and time dependent anomalous fast ion diffusion and MSE-constrained q-profiles to assess fast-ion redistribution/loss effects are reported.

2. Diagnostics for Investigation of MHD-induced Effects on Energetic Ions in NSTX

On NSTX, the amplitude and structure of Alfvén modes are measured using a suite of diagnostics, including Mirnov magnetic coils, ultra soft X-ray (USXR), and reflectometry diagnostics. Neutron yield data supported by Neutral Particle Analyzer (NPA) and scinitillator Fast Ion Loss Probe (sFLIP) diagnostics are used to assess fast-ion redistribution/loss due to MHD-induced effects. Some characteristics of these diagnostics are discussed in this section.

The neutron production in NSTX is predominantly from beam-target reactions as determined by TRANSP calculations. Thus the neutron rate is a robust measure of the energetic ion population and serves as the primary diagnostic for identification of MHD-induced ion redistribution/loss. The energetic ion distributions are measured using the NPA diagnostic. This diagnostic utilizes a PPPL-designed E||B spectrometer [10] which measures the mass-resolved energy spectra of H and D neutrals simultaneously with a time resolution of ~1 ms set by signal-to-noise levels. The calibrated energy range is E = 0.5 – 150 keV and the energy resolution varies from ΔE/E = 3 - 7% from high to low energy. As shown in Fig. 3, the NPA views across the co-injection paths of the three NBI lines on NSTX that inject at major radii R_{NB} of ~ 0.7 m (source A), ~ 0.6 m (source B) and ~ 0.5 m (source C) and can be scanned

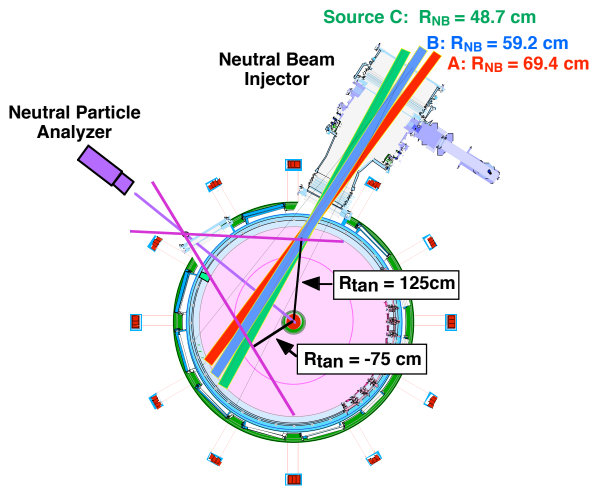

Fig. 3 Layout of the NPA diagnostic on NSTX.

horizontally over a wide range of tangency radii on a shot-to-shot basis. In NSTX, by convention the neutral beam tangency radii are positive for *injection* in the co-direction. On the other hand, the convention adopted for the NPA is that positive sightline tangency radii correspond to *viewing* co-directed ions.

Spatial localization of the NPA flux arises from the intersection of the diagnostic sightline with the NBI sources as illustrated in Fig. 4. The inset in the left panel of this figure shows TRANSP calculation of the charge exchange emissivity for 60 keV deuterium ion energy and a sightline tangency radius of R_{tan} = 0.7 m (blue curve) overlaid with the total beam neutral density for Source A (red curve). The curves are plotted as a function of distance along the NPA sightline measured from the pivot point of the diagnostic (see Fig. 3). Also shown is the pitch angle variation along the sightline (black curve). As can be seen, the charge exchange emissivity is significantly localized due to charge exchange on the beam primary and halo neutrals. In this case, approximately 2/3 of the integrated flux originates from the intersection of the NPA sightline with the NB region where ions are born on passing orbits. The remainder originates in the outboard regions of the plasma where ions are more likely to be deposited on trapped orbits. The pitch angle 'range' sampled by the NPA is obtained from this plot by noting the values of the pitch angle at the rising and falling edges of the beam neutral density curve.

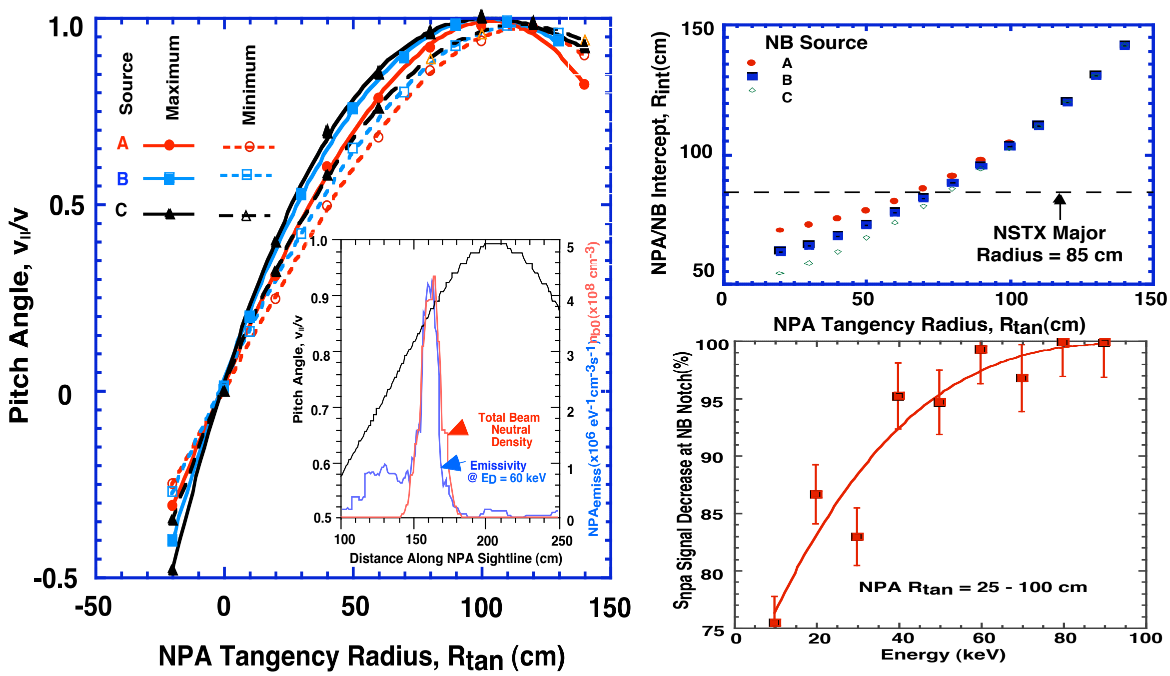

Fig. 4 Pitch angle (left panel) and spatial (upper right panel) localization of the NPA flux arises from the intersection of the diagnostic sightline with the NB sources. Localization is strongest near the NB full energy, but remains substantial over the entire slowing down distribution.

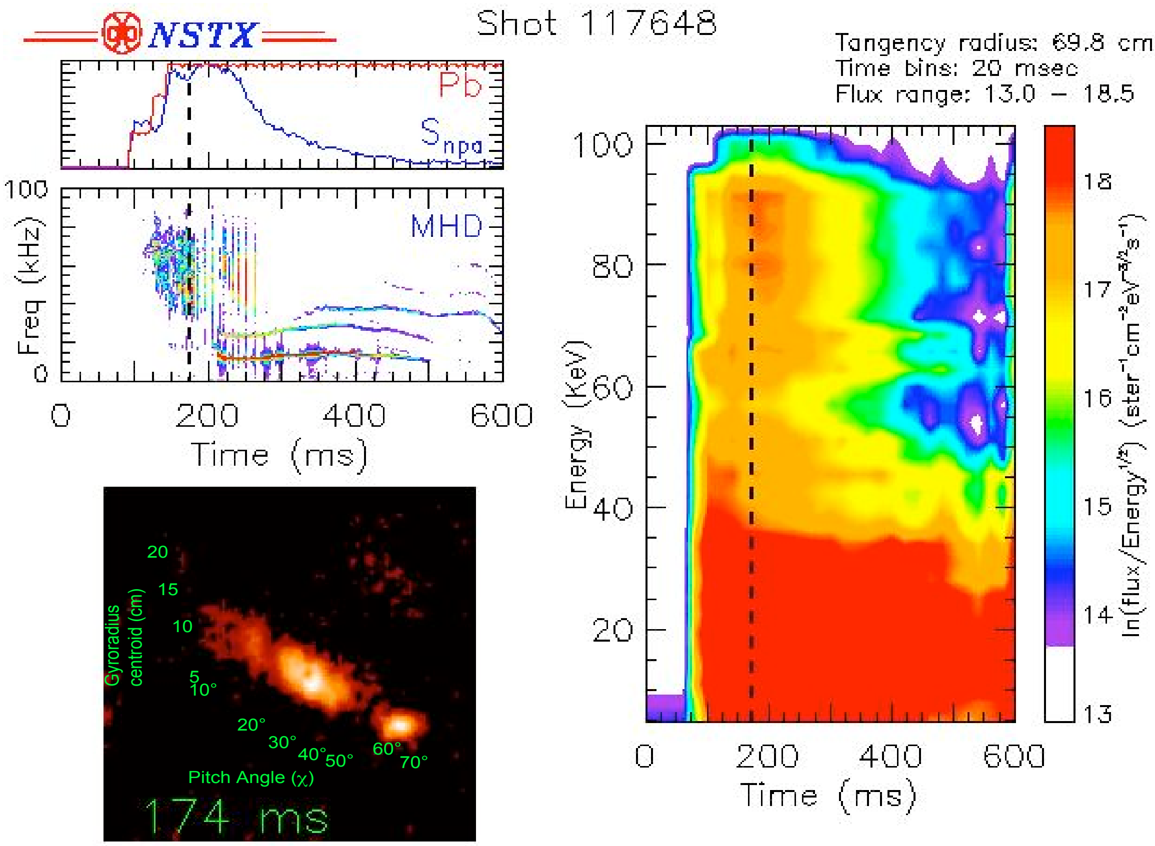

Fig. 5 Example of a display for correlating sFLIP ion loss images (lower left panel) with discharge waveforms and the Mirnov spectrogram (upper left panel) and evolution of the NPA energetic ion distribution (right panel). In AVI mode, the dashed cursor advances with the sFLIP images.

This process was repeated for Sources B and C and for other NPA tangency radii to obtain the curves shown. This spatial localization weakens at smaller NPA tangency radii, R_{tan}, due to attenuation of the beam neutral density with increasing penetration distance. The upper right panel shows the spatial localization of the NPA measurement in terms of the major radius of the intersection of the NPA sightline with the NB axis. Localization is strongest near the NBI full energy, but remains substantial over the entire slowing down distribution (lower right panel).

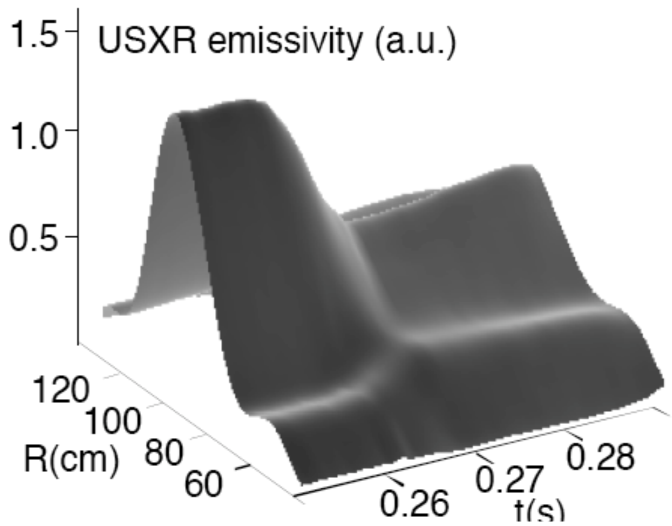

Fig. 6. Illustration of USXR measurements that can be utilized for spatial localization of MHD activity.

Both the volume-integrated neutron and the line-integrated NPA diagnostics show signal depletion due to fast-ion driven instabilities, but cannot distinguish between fast-ion redistribution and loss. Two recently implemented diagnostics on NSTX, the Motional Stark Effect (MSE) and scintillator Fast Lost Ion Probe (sFLIP), facilitate separation of redistribution and loss effects. In particular, sFLIP measures the pitch and energy of fast ions that are ejected from the plasma and intercept the wall-mounted probe thus discriminating fast-ion loss versus redistribution. For certain

H-mode discharges where NPA measurements of the NBI energetic ion spectra exhibit MHD-induced fast-ion depletion, the sFLIP data confirm the existence of an ion loss that occurs primarily for passing particles near the NBI full injection energy (Fig. 5).

3. Bursting MHD Mode Results

Significant fast ion losses are seen in many NSTX shots correlated with 'bursting' EPM and TAE modes as well as fishbone and sawtooth activity. Bursting modes that exhibit rapid downward frequency shifts (chirping) on the time scale of a few milliseconds or less are a characteristic feature of EPM modes. The modes can chirp because the frequency is determined by the fast-ion distribution function, which can be directly modified by the modes rather than thermal plasma parameters. An example of such activity is shown in Fig. 7 where cyclic neutron rate drops of order 5 – 10% associated with the destabilization of EPMs occur. The NPA deuterium energy spectra show the strongest particle density modulation below the NBI half-energy and the density modulation of the highest energy ions is roughly 10%.

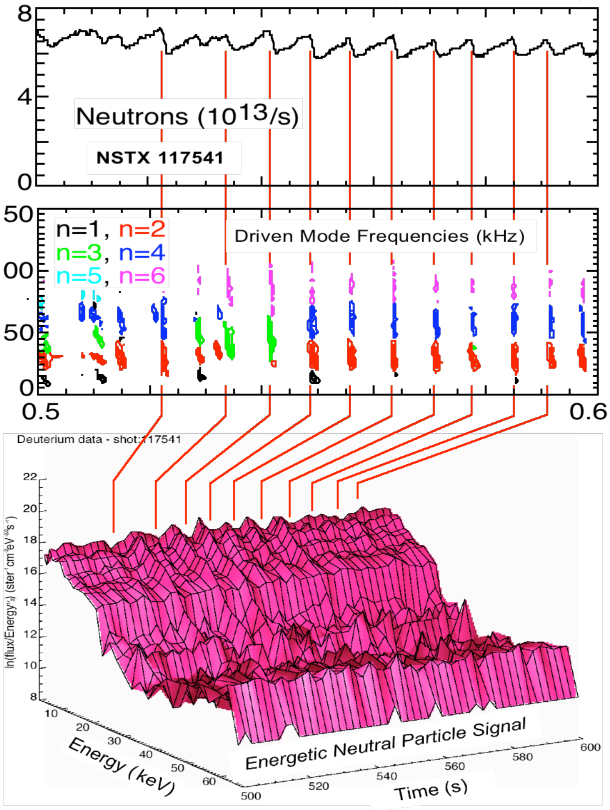

Fig. 7 Illustration of neutron loss (upper panel) due to bursting EPM activity (center panel) and associated spikes in the NPA energetic ion spectrum that occur primarily at lower energies.

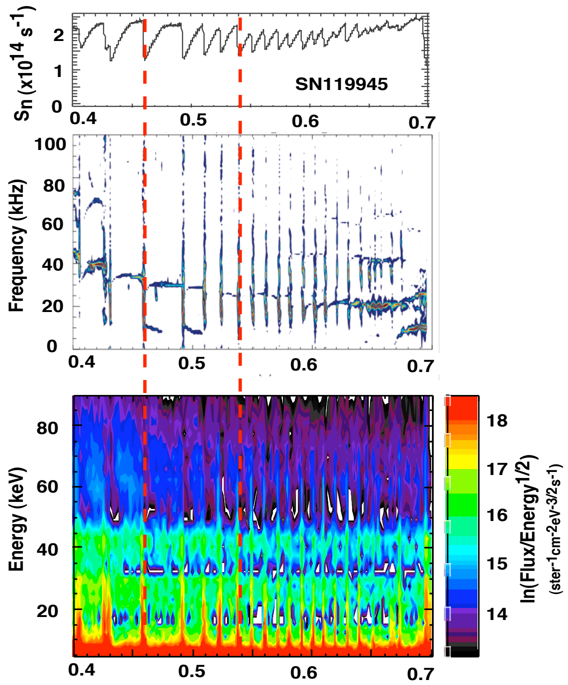

Fig. 8 Illustration of neutron loss (upper panel) due to sawtooth activity (center panel) and associated spikes in the NPA energetic ion spectrum that occur at all energies.

While drops in the neutron rate approaching 40% are seen with some fishbone events [11], in many cases the neutron rate is virtually unaffected. From TRANSP modeling results, large neutron-rate drops generally indicate the loss from the plasma of a substantial fraction of the most energetic fast ions that are responsible for most of the neutron production. Smaller neutron-rate drops could indicate either that the fast ions are just redistributed within the plasma, or that only the lower energy fast ions are expelled. An example of MHD-induced loss due to sawtooth activity is shown in Fig. 8. In contrast to EPM bursts, sawteeth can produce drops in the neutron rate exceeding 50% and in severe cases can cause disruption of the

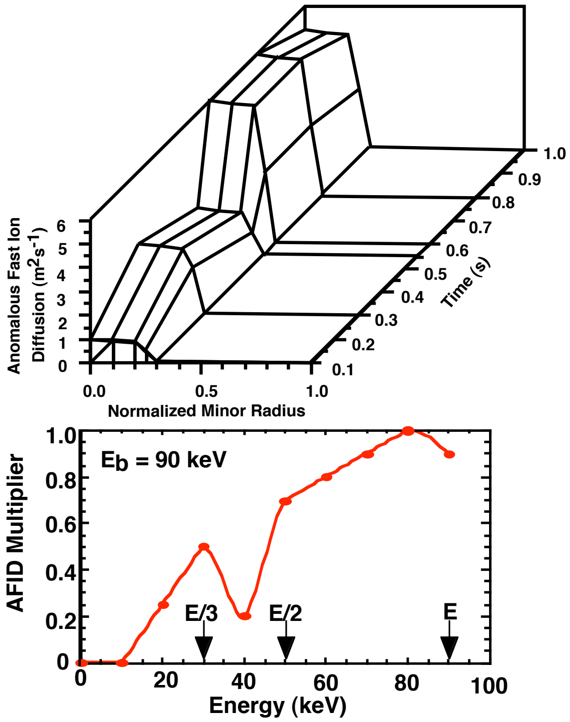

Fig. 9. Illustration of the parameters utilized for the TRANSP anomalous fast ion diffusion model.

discharge. Also, the associated spikes in the NPA flux (lower panel) extend over all energies. The sFLIP images (not shown) clearly indicate that the fast ions are expelled rather than redistributed.

4. Continuous MHD Mode Results

Unlike bursting MHD activity, continuous MHD persists over 100s of milliseconds during which time plasma parameters such as n_e, Z_{eff}, and plasma equilibria usually evolve significantly. This drives changes, for example, in the neutron rate, NPA measurements and sometimes even the nature of the MHD activity itself. The observed depletion of the NPA signal is a combination two effects: changes in the charge exchange emissivity driven primarily by the n_e evolution and MHD-induced fast ion effects. The TRANSP NPA diagnostic simulation is used to correct for the emissivity component leaving a 'residual' depletion attributed to MHD effects. In TRANSP, an Anomalous Fast Ion Diffusion (AFID) model can be applied to simulate MHD-induced redistribution/loss of slowing down ions from NBI. In this model the diffusivity can be specified as a function of time and space in the discharge corresponding to localization of the MHD activity as shown in the upper panel of Fig. 9 as well as over a specified ion energy range to accommodate the energy-selective loss observed in the NPA measurements as shown in the lower panel. Two criteria were employed for determining the fast ion diffusion parameters: the first was to match the measured neutron rate and NPA signal evolution with the TRANSP simulation, and the second was to simultaneously obtain agreement with the measured NPA energetic ion distribution.

Note that energetic ion diffusion is generally small in conventional tokamaks [12] and there is no evidence so far that this is not the case in spherical tokamaks as well. So the use of enhanced energetic ion diffusion to emulate the observed MHD ion loss must not be construed as implying that elevated energetic ion diffusion is a feature unique to spherical tokamaks.

In Fig. 10, the NPA energetic ion spectrum for the selected discharge 117449 shows significant flux depletion above $E_b/2$ (encircled region) where E_b = 90 keV is the

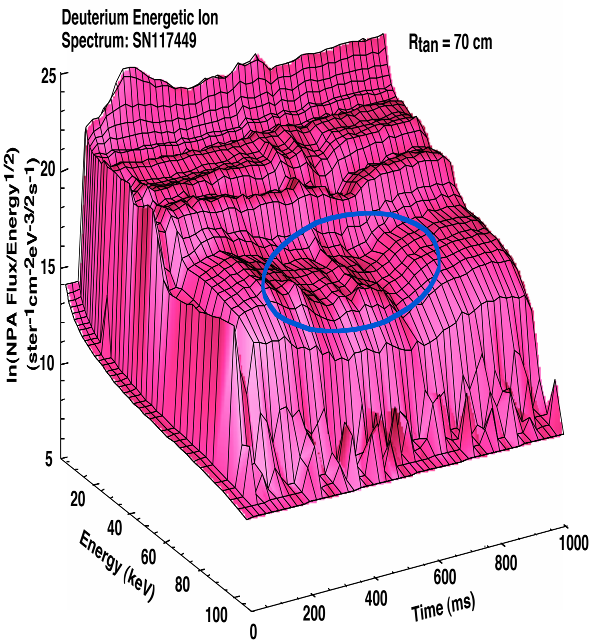

Fig.10. Illustration of the NPA energetic ion spectrum for SN117449 showing depletion of the measured flux primarily above $E_b/2$.

NBI energy. A smaller depletion occurs around $E_b/3$. Onset of the depletion correlates with onset of strong TAE activity at t ~ 0.2 s.

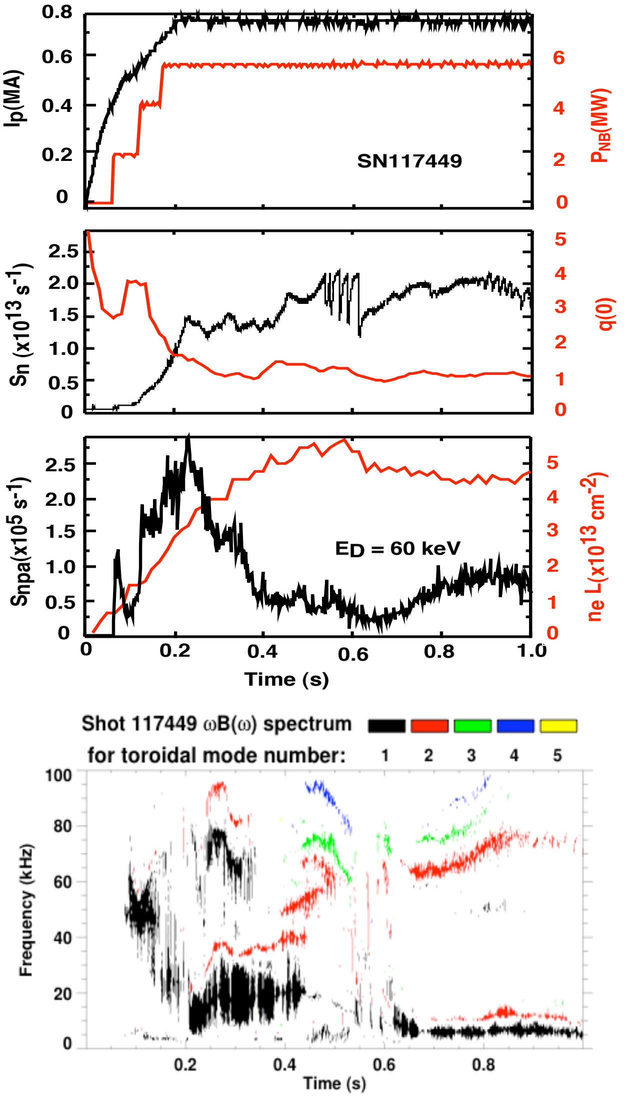

Fig. 11 Selected plasma waveforms and Mirnov spectrogram for discharge 117449.

The waveforms for this discharge shown in Fig. 11 are, from the top, I_p and total NBI power, neutron rate and core safety factor, NPA signal at E_d = 60 keV and electron line density, and finally the Mirnov MHD spectrogram. Depletion of the NPA signal commences at ~ 0.2 s concurrent with onset of TAE activity and continues through bursting EPM activity around 0.5 – 0.6 s and n = 1, f ~ 10 kHz kink-type MHD beyond ~ 0.6 s. A modest recovery of the NPA signal after 0.6 s occurs because a drop in n_e slightly relaxes the emissivity contribution to the depletion.

The TRANSP analysis results are shown in Figs. 12 for the neutron rate (left panel) and NPA signal (right panel). Without AFID the TRANSP calculations are well above measurements. However, the calculations with AFID agree reasonably well with measurements, particularly during the time of interest from 0.6 – 1.0 s. Simultaneously, good agreement between measured and simulated NPA energetic ion spectra is obtained as shown in Fig. 13.

The effect of MHD-induced energetic ion redistribution on plasma current density profiles is assessed by comparing measured and calculated current profiles as shown in

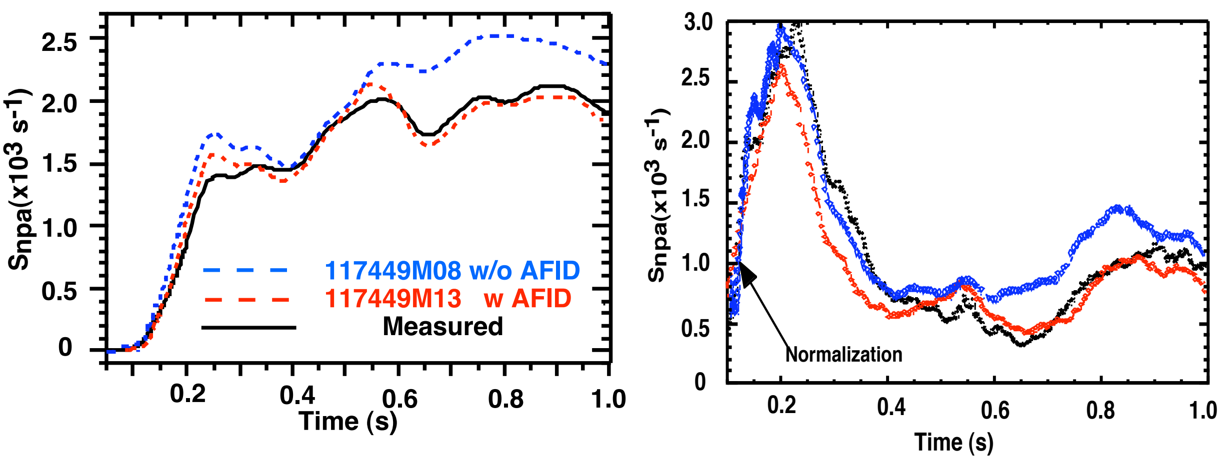

Fig. 12 Shown are results of TRANSP simulation using anomalous fast ion diffusion for discharge 117449. Black lines are measurements and red/blue lines are TRANSP simulations with/without anomalous fast ion diffusion. The time of interest is 0.6 – 1.0 s.

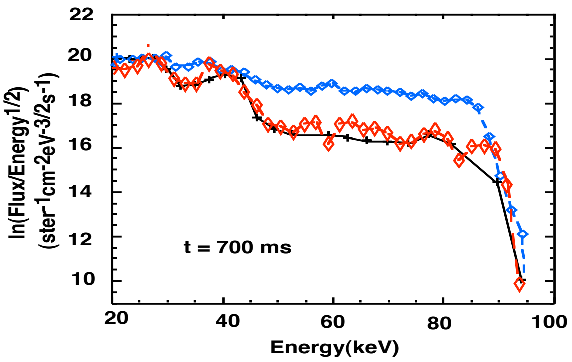

Fig. 13 Matching of the measured energetic ion distribution with TRANSP AFID model.

Fig. 14. An equilibrium code is used to compute the inductive (orange) and bootstrap (red) current profile components as described in [8]. The NBICD component (blue) from TRANSP calculation and the summation of the aforementioned components yields the calculated total (black) toroidal current profile. The measured current profile (gray) is derived from a MSE-constrained reconstruction that uses the CHERS radial electric field profile from carbon impurity force balance to correct the MSE pitch angle data.

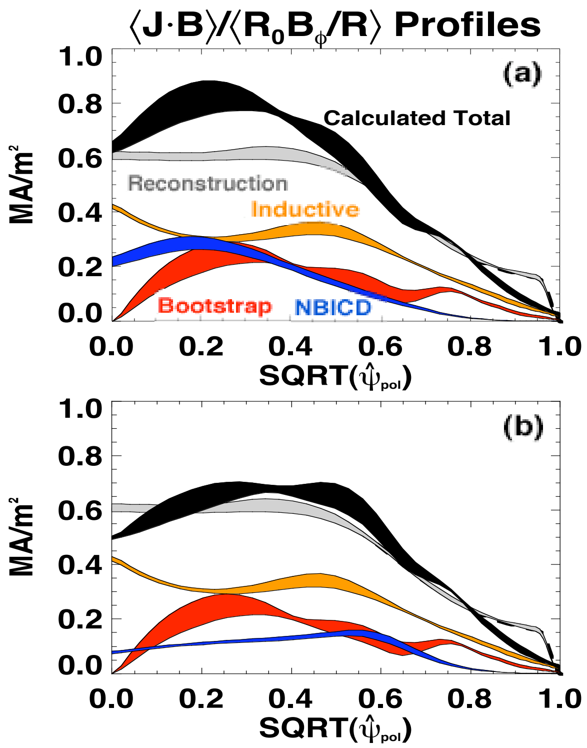

Fig. 14 Matching MSE-reconstructed and calculated current profiles using AFID in TRANSP for NBICD redistribution.

In Fig. 14(a), it can be seen that the calculated total current density exceeds the MSE-reconstruction value by ~ 25% in the core region. However, as shown in Fig. 14(b), the TRANSP-calculated redistribution of fast ions using the AFID model reduces the NBICD component and hence the calculated total current density in the core to essentially the same value as the MSE reconstruction.

In summary, MHD activity can reduce the neutron rate, modify the measured NPA efflux and induce NBICD profile redistribution. TRANSP analysis using AFID models these effects and can yield agreement between the calculated total current profile and that from MSE-constrained reconstruction.

5. Acknowledgements

This work was supported by U.S. DOE Contract DE-AC02-76CH03073 and Grant DE-FG02-99ER54523 (JHU).

6. References

[1] C. Z. Cheng and M. S. Chance, Phys. Fluids **29**, (1986) 2471
[2] E. D. Fredrickson, N. N. Gorelenkov, D. Darrow, *et al.*, Phys. of Plasmas **10** (2003) 2852
[3] H. L. Berk, B. N. Breizman, J. Candy, *et al.*, Phys. Plasmas **6**, (1996) 3102
[4] E. D. Fredrickson, *et al.*, 20th IAEA Fusion Energy Conference, Vilamoura, Portugal, 1-6 November 2004 (IAEA, Vienna) CD-ROM EX/5-3
[5] S. S. Medley, *et al.*, Nucl. Fusion **44**, (2004) 1158
[6] W. W. Heidbrink, N. N. Gorelenkkov, M. Murakami, Nucl. Fusion **42**, (2002) 972
[7] K. L. Wong, *et al.*, Nucl. Fusion **45**, (2005) 30
[8] J. E. Menard, *et al.*, Phys. Rev. Lett. **97**, (2006) 095022
[9] R. V. Budny, Nucl. Fusion **34**, (1994) 1247
[10] S. S. Medley and A. L. Roquemore, Rev. Sci. Instrum. **69**, (1998) 2651
[11] E. D. Fredrickson, L. Chen, R. B. White, Nucl. Fusion **43**, (2003) 1258
[12] W. W. Heidbrink and G. J. Sadler, Nucl. Fusion **34**, (1994) 535